

Quantitative measure of tetrahedral- sp^3 geometries in amorphous phase-change alloys

M. Micoulaut*

Laboratoire de Physique Théorique de la Matière Condensée, Université Pierre et Marie Curie, 4 Place Jussieu, F-75252 Paris Cedex 05, France

K. Gunasekera, S. Ravindren, and P. Boolchand

School of Electronics and Computing Systems, College of Engineering and Applied Science, University of Cincinnati Cincinnati, Ohio 45221-0030, USA

(Received 17 February 2014; revised manuscript received 3 September 2014; published 24 September 2014)

Phase change or Ovonic memory technology has gained much interest in the past decade as a viable solution for the rapid increase in the demand for memory storage. This unique technology, first proposed by S. Ovshinsky in 1968, is based on storing information on the crystalline and amorphous phases of a material. The most common phase-change materials (PCMs) use chalcogenide alloys such as the $\text{Ge}_2\text{Sb}_2\text{Te}_5$ (GST225). However, while the structure of its crystalline phase is relatively well characterized as consisting of a rhombohedrally distorted rock-salt lattice, the corresponding amorphous phase remains still poorly understood. Here, we show that ^{119}Sn Mössbauer spectroscopy and angular constraint counting of simulated structures can provide a quantitative measure of the sp^3 tetrahedral fraction of Ge or Si cation in amorphous phase-change binary tellurides $\text{Ge}_x\text{Te}_{1-x}$ and $\text{Si}_x\text{Te}_{1-x}$. This represents the first quantitative estimate of such local structures, and reveals the fraction to be nearly 50%, while also revealing implications for the phase-change mechanism itself.

DOI: [10.1103/PhysRevB.90.094207](https://doi.org/10.1103/PhysRevB.90.094207)

PACS number(s): 61.43.Fs

I. INTRODUCTION

Phase change phenomenon involves a transition between a crystalline conducting state and an amorphous semiconducting one [1,2], with attendant changes in electronic density of states and band gap. It has, therefore, been recognized that typical structural motifs (tetrahedra, octahedra) should play an important role in phase switching phenomena because of a change in the nature of chemical bonding reflected by different electronic orbitals. The sp^3 hybridized tetrahedra, typical of covalent semiconductors, involve, for instance, only s electrons whereas an octahedral (s, p) bonding facilitates conduction. The local structure of such phase-change tellurides has been revealed from extended x-ray absorption fine structure (EXAFS) experiments [3,4], and it was found that Ge atoms actually switch from a sixfold octahedral coordination in the crystalline phase to a fourfold coordination in an amorphous one.

The nature of this fourfold Ge, whether a pyramidal (i.e., “defect-octahedral,” DO) or a tetrahedral (T) unit, and its fraction, has been debated, and still remains unresolved. In addition, some conclusions based on EXAFS [5] and reverse Monte Carlo simulations [6] have contradicted each other [3,4]. This may simply result from uncontrolled sample processing [7] or deposition methods [8,9], which can dramatically affect the physical behavior including the local structure. First-principles molecular dynamics (FPMD) simulations have been used to provide additional information [10–13] on the atomic coordination and geometry, and these have shown that the Te coordination is larger than 2, whereas most of Ge is fourfold with a finite fraction being sp^3 tetrahedral. However, the way this fraction is computed remains largely qualitative. Akola and Jones [10] assign tetrahedral character if all Ge-centred bond angles are greater than 100° but this

must obviously give rise to some uncertainties given that the bond angles involved in the two geometries (DO and T, 90° and 109°) are close, and display distributions leading to a possible overlap. Alternatively, Raty and co-workers [11] used a bond-length argument in $\text{Ge}_1\text{Sb}_2\text{Te}_4$, remarking that the fourth-neighbor distribution of a Ge atom is bimodal, depending on whether it is three- or four-fold (tetrahedrally) coordinated. Finally, Caravati *et al.* [13] calculate a local order orientational parameter distribution that reveals tetrahedral character [14] but the integration of this distribution that yields the estimate depends unfortunately on the integration boundaries. Fingerprints of tetrahedral geometries have also been recently provided using either simulated Raman spectra [15] or x-ray absorption-near-edge-structure spectroscopy [16] but the question of finding an explicit signature, and a quantitative measure of sp^3 tetrahedral Ge as a function of thermodynamic conditions (e.g., composition) in phase-change tellurides remains a largely open issue.

In the present contribution, we address the *central* question of the nature of structural motifs and chemical bonding by investigating two binary amorphous tellurides, $\text{Ge}_x\text{Te}_{1-x}$ and $\text{Si}_x\text{Te}_{1-x}$ with $x \leq 20\%$. We propose two new methods in the context of phase-change materials, an experimental and a theoretical one, that can determine without ambiguity the nature of the local structures (different geometry), their fraction, and their evolution under moderate compositional changes in the amorphous phase. We rely on ^{119}Sn Mössbauer spectroscopy that allows for a detection of local structures *via* the nuclear hyperfine structure [17] (δ -isomer shift, and Δ -quadrupole splitting), and leads to a direct observation of site geometry. For the theory part, we use first-principles molecular dynamics (FPMD) simulations, in conjunction with topological constraint counting. Compared to previous experimental and theoretical studies, the present results mark compelling progress in the characterization of the topology of phase-change materials given that, ultimately, it is the

*Corresponding author: mmi@lptl.jussieu.fr

signature of local structures and their fraction that controls functionality. We find that at low Ge and Si content ($x = 14\%$ – 15%), both Si-Te and Ge-Te binary are dominated by sp^3 tetrahedral fractions in the 55%–70% range. However, with only a slight increase of $x = 18\%$, in the Ge-Te binary, the sp^3 tetrahedral fraction dramatically lowers to near 42% with Ge atoms predominantly found in an octahedral geometry. On the other hand, in the Si-Te binary, the sp^3 tetrahedral fraction displays the opposite behavior, and increases up to $\simeq 92\%$ for $x = 20\%$. These estimates established from a direct measurement (Mössbauer spectroscopy), and qualitatively recovered from the simulation, unravels the central role played by sp^3 tetrahedral motifs and provides, given the abundance of such structural motifs, indirect support to phenomenological models of the phase-change phenomenon [3]. Taken together, the results allow reconsidering in a rather deep and quantitative fashion the local structure of amorphous tellurides, while also revealing important implications for the phase-change mechanism itself.

The paper is organized as follows. In Sec. II, we give the details about the sample synthesis and the measurements made, and describe the electronic modeling. In Sec. III, we provide the structural results of our model Si-Te and Ge-Te alloys and calculate the fraction of tetrahedral Ge/Si in Sec. IV, which is compared to the measurements from Mössbauer spectroscopy. We then discuss the broad consequences of our findings in the context of the phase-change phenomena.

II. METHODS

A. Experimental

The low optical gap of the tellurides makes optical characterization [18,19] by Raman scattering challenging. In our work we used calorimetric reversibility windows as a measure of melt/glass homogeneity. We first synthesized ternary $\text{Ge}_x\text{Si}_x\text{Te}_{100-2x}$ bulk glasses [20] by reacting the pure elements at the temperature of 950 °C in evacuated quartz tubings. In such ternary bulk glasses when reacted for 7 days, calorimetric measurements showed evidence of a broad enthalpic reversibility window. However, that reversibility window in this ternary became a square well like when these melts were reacted for 14 days. Indeed, the appearance of a reversibility window with sharp edges is the hallmark of melt homogenization as noted in selenides [18,19] and sulfides [21] of the group IV elements. Guided by these considerations, we synthesized binary Ge-Te and Si-Te glasses for the present work by reacting the pure elements at 950 °C in evacuated quartz tubes for 14 days. The batch size was kept at 0.5 gram as in the experiments on the Ge-Si-Te ternary.

1. Calorimetric properties

For the present Ge-Te and Si-Te systems, the results of the reversing heat flow measurements using a TA Instruments model MDSC-2920 are given in Table I. The MDSC instrument was calibrated for temperature, enthalpy, and specific heat using In and Pb and Sapphire standards. Glasses of $\simeq 20$ mg were hermetically sealed in aluminium pans. Heat flow measurements were carried out at a scan rate of 3 °C/min, modulation amplitude of 1 °C and a period of 100 s. The

TABLE I. Calorimetric measured glass transition temperatures T_g and heat capacity jump ΔC_p near T_g in Ge-Te and Si-Te glasses with composition.

	$\text{Ge}_{15}\text{Te}_{85}$	$\text{Ge}_{17}\text{Te}_{83}$	$\text{Ge}_{18}\text{Te}_{82}$
T_g (°C)	134.5	146.4	153.0
ΔC_p (cal/g/K)	0.012(1)	0.011(5)	0.023(0)
	$\text{Si}_{14}\text{Te}_{86}$	$\text{Si}_{16}\text{Te}_{84}$	$\text{Si}_{18}\text{Te}_{82}$
T_g (°C)	138.6	147.8	152.0
ΔC_p (cal/g/K)	0.015(8)	0.016(0)	0.018(0)

glass transition T_g and the heat capacity jump ΔC_p at the glass transition were extracted from the reversing heat flow component, T_g was extracted from the inflection point, and ΔC_p from the step height in heat capacity.

2. Mössbauer spectroscopy

To the best of our knowledge, previous investigations using this technique in tellurides have been reported only for selected compositions of Si-Te glasses [22] using ^{125}Te and ^{129}I substitution. Here one uses ^{119}Sn Mössbauer spectroscopy. A $\text{Ca}^{119}\text{SnO}_3$ source of 23.8-keV γ ray was used to excite the nuclear resonance using a constant acceleration drive. The emitter and glass sample absorber were cooled to 78 K in a He exchange gas dewar. Observed spectral lineshapes were deconvoluted in singlets and doublets to extract the isomer shift δ and quadrupole splitting Δ (Table II). All spectra in Ge-Te and Si-Te glasses were analyzed and their isomer shift δ are compared to reference compounds (Fig. 1) having either a tetrahedral geometry (c-Si, sp^3) or an octahedral geometry (SnTe , Sn^{2+}).

It is important to emphasize that the ^{119}Sn Mössbauer experiments used a 1 wt.% alloy in Sn metal of the glass of interest (Si-Te or Ge-Te), but the Sn metal used was enriched to nearly 100% in ^{119}Sn , the resonant isotope. To see a respectable signal in this spectroscopy, one typically needs 0.1 to 0.5 mg of

TABLE II. ^{119}Sn Mössbauer effect parameters of tetrahedral (T) and defect octahedral (DO) sites. Isomer shift δ , quadrupole splitting Δ (for DO geometry), and full width at half maximum (FWHM) in Ge-Te and Si-Te glasses with changing content. The errors in δ , Δ , and FWHM are 0.02, 0.03, and 0.03 mm/s, respectively.

		$\text{Ge}_{15}\text{Te}_{85}$	$\text{Ge}_{17}\text{Te}_{83}$	$\text{Ge}_{18}\text{Te}_{82}$
δ (mm/s)	T	1.97	1.95	1.98
	DO	3.17	3.20	3.24
Δ (mm/s)		0.78	0.85	0.73
FWHM (mm/s)	T	0.99	1.00	1.06
	DO	1.02	0.99	0.98
		$\text{Si}_{14}\text{Te}_{86}$	$\text{Si}_{16}\text{Te}_{84}$	$\text{Si}_{18}\text{Te}_{82}$
δ (mm/s)	T	1.92	1.92	1.92
	DO	3.24	3.16	3.21
Δ (mm/s)		0.96	1.08	0.99
FWHM (mm/s)	T	1.00	0.98	1.00
	DO	1.07	1.03	0.94

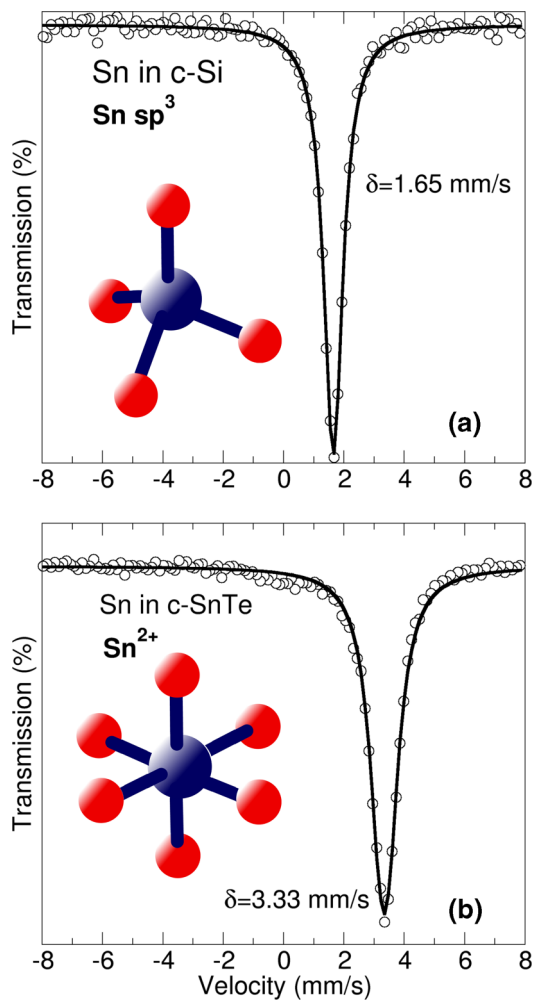


FIG. 1. (Color online) ^{119}Sn Mössbauer spectra of Sn as a dilute impurity in (a) c-Si and (b) c-SnTe. Note that a resonance is observed at $\delta = 1.65 \pm 0.02$ mm/s when Sn is tetrahedrally coordinated, but upshifted to $\delta = 3.33 \pm 0.02$ mm/s when Sn is octahedrally coordinated.

$^{119}\text{Sn}/\text{cm}^2$ in the absorber [17], and in our experiments, carried out at 78 K, we typically saw a 5% resonance effect. With an accumulation of close to 0.5 million counts on the baseline, we thus observed a signal to noise ratio of about 30, which is a rather large signal/noise. This led to rather high-quality Mössbauer spectra, even for the compounds having the lowest fraction of group IV atoms ($\text{Ge}_{15}\text{Te}_{85}$ and $\text{Si}_{14}\text{Te}_{86}$).

B. Molecular dynamics

CPMD simulations using the CPMD program [23] were performed at constant volume on five systems $\text{Ge}_{10}\text{Te}_{90}$, $\text{Ge}_{15}\text{Te}_{85}$, $\text{Ge}_{20}\text{Te}_{80}$, $\text{Si}_{14}\text{Te}_{84}$, and $\text{Si}_{20}\text{Te}_{80}$ containing 200 atoms positioned in a periodically repeated cubic cell whose size allows recovering the experimental densities of the low-temperature liquids [24,25], and selected liquid temperatures (700, 820, and 920 K). Note that the $\text{Si}_{14}\text{Te}_{86}$ compound was simulated using the density of a 15% Si, the selection of a 14% being performed in order to be directly comparable with the experimental Mössbauer results. The differences in densities

are small [24], and led to pressures in the amorphous phase that were found between -1.0 GPa and 0.5 GPa.

A generalized gradient approximation was used, using an improved scheme for the exchange-correlation energy obtained by Perdew, Burke, and Ernzerhof (PBEsol) previously validated for the study of elemental tellurium [26], in conjunction with Trouiller-Martins pseudopotentials. Wave functions were expanded at the Γ point of the supercell on a plane wave basis set with an energy cutoff $E_c = 20$ Ry. During the CPMD simulation, a fictitious electron mass of 2000 a.u. and a time step of $\Delta t = 0.12$ fs has been used to integrate the equations of motion. In addition, we used an (attractive) empirical dispersion coefficient (Grimme) correction [27] that has been shown to substantially improve the structural properties of Ge-Te alloys, and increase the agreement with experimental data [28]. This (attractive) correction [27] is given by

$$E_{\text{disp}} = -s_6 \sum_{i=1}^{N-1} \sum_{j=i+1}^N \frac{C_{ij}}{R_{ij}^6} f_{\text{dmp}}(R_{ij}), \quad (1)$$

where N is the number of atoms of the system, C_{ij} is the dispersion coefficient for atom pair ij and R_{ij} is the interatomic distance. A damping function [27] $f_{\text{dmp}}(R_{ij}) = [1 + \exp(-d(R_{ij}/R_c - 1))]^{-1}$ has been also used in order to avoid singularities at short interatomic distances. Here, R_c is a cutoff distance canceling E_{disp} for $R_{ij} < R_c$. Parameters for the Ge-Te systems (R_c , C_{ij} , d_{ij}) are given in Ref. [28], and for the Si-Te system, one furthermore has $C_{ij} = 95.43$ and $176.97 \text{ eV } \text{\AA}^{-6}$, and $R_{ij} = 3.43$ and 3.44 \AA for Si-Si and Si-Te pairs, respectively [27].

One of the main results of taking into account such an empirical term is that an increased agreement on structure is obtained, which solves the well-known bond distance problem encountered in standard DFT-based simulations of tellurides [12]. This leads indeed to a reduction of the coordination numbers and a better reproduction of the experimental pair distribution function $g(r)$ as also demonstrated recently in the liquid phase for the present investigated Ge-Te compositions [29], as discussed next.

III. STRUCTURE

In Fig. 2, we represent the total pair correlation function $g(r)$ for the different glasses of interest. These calculated quantities are compared to available experimental data from neutron diffraction [30]. First, we remark that the overall agreement between simulation and experiment is very good as exemplified for $\text{Ge}_{15}\text{Te}_{85}$ and $\text{Ge}_{20}\text{Te}_{80}$, and certainly improved when dispersion forces using Eq. (1) are treated during simulation. For the $\text{Ge}_{20}\text{Te}_{80}$ compound, a direct comparison with the experimental data [30,31] shows that while the position of the first peak located at 2.69 \AA in the experimental pair correlation function $g(r)$ is rather well reproduced without the Grimme correction (green curve), the broadening of the first peak and a reduced structuration (minimum at $\simeq 3.3\text{--}3.4 \text{ \AA}$) will automatically lead to coordination numbers that are overestimated with respect to an experimental estimate [30] or a reverse Monte Carlo

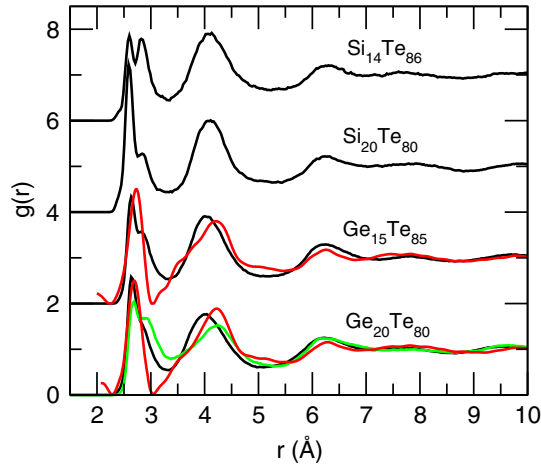


FIG. 2. (Color online) Calculated total pair correlation function $g(r)$ of $\text{Ge}_{15}\text{Te}_{85}$, $\text{Ge}_{20}\text{Te}_{80}$, $\text{Si}_{14}\text{Te}_{86}$, and $\text{Si}_{20}\text{Te}_{80}$, compared to the corresponding experimental function from neutron diffraction (red, Ref. [30]). The green curve corresponds to a simulation that does not take into account the correction (Eq. (1)) due to dispersion forces [27].

analysis [32]. Definitely, the correction (1) improves the structural description of the short range order.

The detail of the partial pair correlation functions g_{ij} of $\text{Ge}_{20}\text{Te}_{80}$, $\text{Si}_{14}\text{Te}_{86}$, and $\text{Si}_{20}\text{Te}_{80}$ is shown in Fig. 3. For the partial pair-correlation functions of $\text{Ge}_{20}\text{Te}_{80}$, we find results that are very similar to those reported for liquid $\text{Ge}_{15}\text{Te}_{85}$ [28] but with peaks that have sharpened and with well-defined shells of neighbors as compared to the liquid. The calculated bond distances are actually very close to those determined from a reverse Monte Carlo (RMC) fitting of the total pair correlation function given that we find the bond distances $r_{\text{GeGe}} = 2.48 \text{ \AA}$, $r_{\text{GeTe}} = 2.64 \text{ \AA}$, and $r_{\text{TeTe}} = 2.90 \text{ \AA}$, to be compared with 2.50, 2.60, and 2.76 \AA [11]. Similar conclusions can be drawn for the global shape of the partials g_{ij} , although it should be noted that the RMC determined Te-Te pair correlation function is much more structured as the one represented in Fig. 3. However, a partial experimental determination of the g_{ij} 's for liquid $\text{Ge}_{15}\text{Te}_{85}$ [28] shows that the agreement between simulation [28] and experiment is quite close. Our calculated bond distances also agree with a determination from extended x-ray absorption fine structure (EXAFS) measurements which found [33] $r_{\text{GeTe}} = 2.59 \pm 0.02 \text{ \AA}$, and $r_{\text{TeTe}} = 2.74 \pm 0.02 \text{ \AA}$.

We furthermore note from the shape of the partial pair correlation functions that the Si-Te alloys are somewhat more structured given that $g_{\text{Si-Te}}$ decays to zero after the first shell of neighbors, similar to archetypal oxide or chalcogenide glasses [34].

Figure 4 shows the bond angle distributions Te-Te-Te and Te-Te- X with $X = \text{Ge}$ and Si for $\text{Ge}_{20}\text{Te}_{80}$ (black) and $\text{Si}_{20}\text{Te}_{80}$ (red). Weak differences are found with changing Ge/Si composition (not shown). The Te-Te-Te bond angle distribution is found to display the usual features found in liquid or amorphous Te [26], i.e., a main peak at 90° and a contribution at 160° , indicating that Te is predominantly in a defect-octahedral geometry. Small differences are obtained between the Si- and the Ge-based alloys.

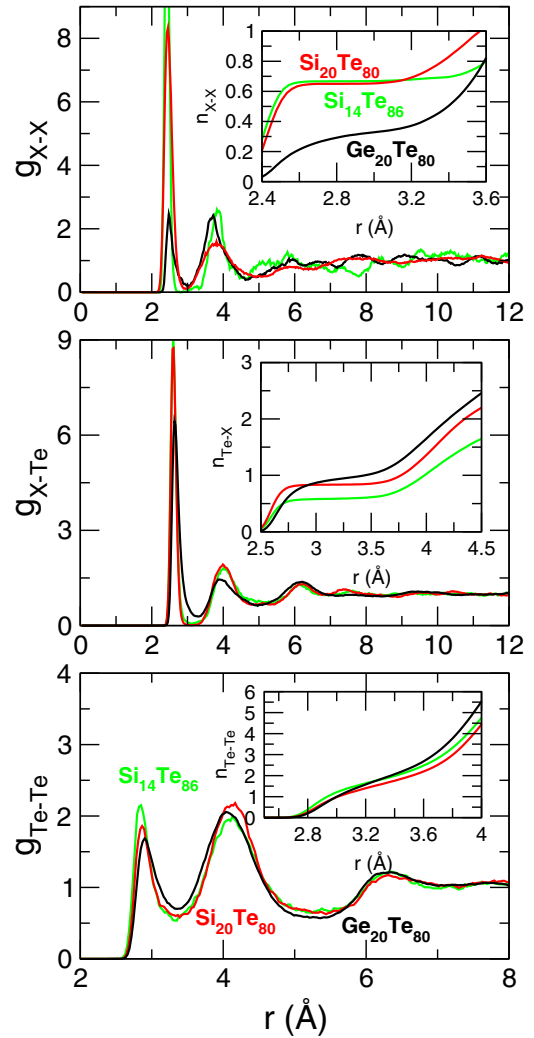


FIG. 3. (Color online) Calculated partial pair correlation functions g_{ij} in $\text{Ge}_{20}\text{Te}_{80}$ (black), $\text{Si}_{14}\text{Te}_{86}$ (green), and $\text{Si}_{20}\text{Te}_{80}$ (red). The inset shows corresponding running coordination numbers $n_{ij}(r)$.

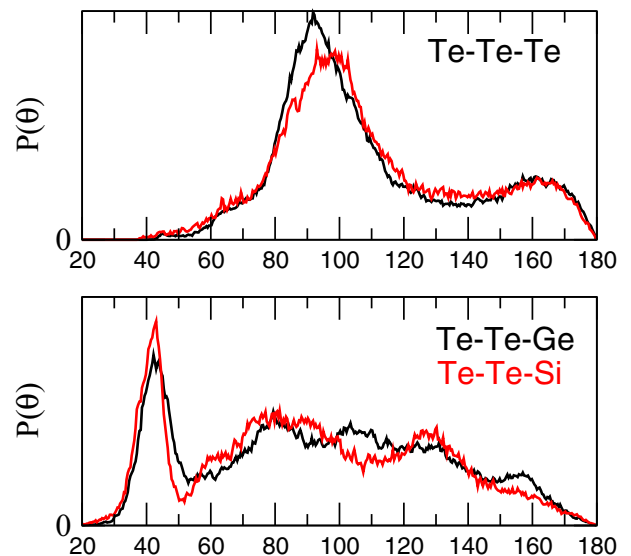


FIG. 4. (Color online) Calculated bond angle distributions Te-Te-Te, Te-Te- X ($X = \text{Ge}$ and Si) in $\text{Ge}_{20}\text{Te}_{80}$ (black) and $\text{Si}_{20}\text{Te}_{80}$ (red).

TABLE III. Calculated partial coordination numbers n_{XX} ($X = \text{Ge}$ and Si), $n_{\text{Te}X}$, and n_{TeTe} , coordination numbers n_X and n_{Te} and average coordination number \bar{r} in amorphous $\text{Ge}_{10}\text{Te}_{90}$, $\text{Ge}_{15}\text{Te}_{85}$, $\text{Ge}_{20}\text{Te}_{80}$, $\text{Si}_{14}\text{Te}_{86}$, and $\text{Si}_{20}\text{Te}_{80}$. All calculations have been computed at the corresponding minimum r_m of the relevant partial pair correlation function. Numbers are given with an error bar of ± 0.05 .

Composition	n_{XX}	$n_{\text{Te}X}$	n_{TeTe}	n_X	n_{Te}	\bar{r}
$\text{Ge}_{10}\text{Te}_{90}$	—	0.48	2.53	4.32	3.01	3.14
$\text{Ge}_{15}\text{Te}_{85}$	0.33	0.65	2.11	4.01	2.76	2.95
$\text{Ge}_{20}\text{Te}_{80}$	0.33	0.96	1.94	4.16	2.90	3.15
$\text{Si}_{14}\text{Te}_{86}$	0.41	0.58	1.89	3.97	2.47	2.68
$\text{Si}_{20}\text{Te}_{80}$	0.65	0.83	1.74	3.99	2.58	2.86

Integration of the partial pair correlation functions at the corresponding minimum r_m (e.g., $r_m = 3.30 \text{ \AA}$ for the Ge-Te pair in $\text{Ge}_{20}\text{Te}_{80}$, see Fig. 3) yields the partial coordination numbers n_{ij} for the alloys, and the species-related ones n_i (Table III). We find that with increasing composition, the Te coordination tends to increase, whereas the group IV coordination number remains nearly constant.

IV. TETRAHEDRAL GERMANIUM

We now turn to the central topic of the work, i.e., methods allowing for a neat estimate of the fraction of tetrahedral group IV atoms.

A. From Mössbauer spectroscopy

We first focus on the experimental signature. The local environment of Ge and Si has been probed using an original characterization technique in the context of phase-change materials - ^{119}Sn Mössbauer spectroscopy [17]. As mentioned earlier, we doped traces ($\approx 1 \text{ wt\%}$) of ^{119}Sn by reacting nearly 100 % isotopically enriched pure elemental Sn in the glass of interest. In trace amounts, *isovalent* Sn will replace Si and Ge local environments in the network, and reproduce the group IV atom local geometry and chemical bonding. When Sn is in a sp^3 -tetrahedral bonded state as a dilute substituent in c-Si, one observes a narrow Mössbauer resonance ($\Gamma = 0.80 \text{ mm/s}$ to be compared with the Heisenberg principle determined natural linewidth of 0.69 mm/s) with unique chemical shift of $\delta = 1.65 \pm 0.02 \text{ mm/s}$ with respect to Sn^{4+} [Fig. 1(a)], this shift being characteristic of tetrahedrally coordinated Sn. Similarly, the Sn^{2+} oxidation state is found in crystalline SnTe which has an octahedral geometry as in GeTe [2], as

TABLE IV. Experimentally measured (Expt.) and calculated (Simul.) fraction η_T (in %) of tetrahedral sites in amorphous Ge-Te and Si-Te with changing group IV atom content.

	$\text{Ge}_{10}\text{Te}_{90}$	$\text{Ge}_{15}\text{Te}_{85}$	$\text{Ge}_{17}\text{Te}_{83}$	$\text{Ge}_{18}\text{Te}_{82}$	$\text{Ge}_{20}\text{Te}_{80}$
Expt.		57.0 ± 1.1	57.9 ± 1.2	41.6 ± 0.8	
Simul.	62.3 ± 3.4	65.4 ± 2.0			54.6 ± 1.6
		$\text{Si}_{14}\text{Te}_{86}$	$\text{Si}_{16}\text{Te}_{84}$	$\text{Si}_{18}\text{Te}_{82}$	$\text{Si}_{20}\text{Te}_{80}$
Expt.		69.9 ± 1.4	73.6 ± 1.5	74.2 ± 1.5	
Simul.		87.3 ± 2.9			91.8 ± 2.8

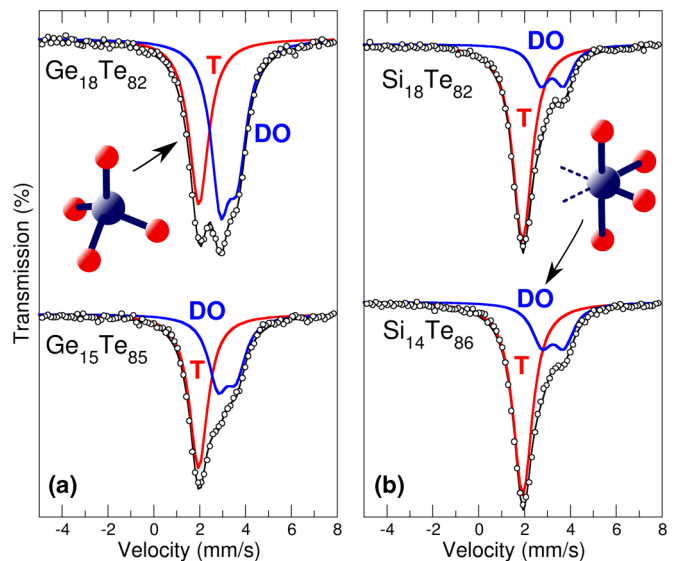


FIG. 5. (Color online) ^{119}Sn Mössbauer spectra of amorphous $\text{Ge}_x\text{Te}_{1-x}$ (a) and $\text{Si}_x\text{Te}_{1-x}$ at selected compositions. According to reference compounds (Fig. 1), spectra can be deconvoluted into two sites T, tetrahedral (red), and DO, defect octahedral (pyramidal, blue), the latter being schematically represented in panel (b) by an octahedral site with two vacancies.

revealed by a Mössbauer resonance at an isomer shift of $\delta = 3.33 \pm 0.02 \text{ mm/s}$ [Fig. 1(b)]. Furthermore, since there are no vacancies in this perfect rocksalt-type structure of the two Sn and Te sublattices, no quadrupole splitting is observed [17], which indicates presence of an octahedral coordination, i.e., the absence of vacancies in the immediate environment of Sn.

Figure 5 shows the Mössbauer spectra of two selected compositions in each telluride system, and these can be deconvoluted into a singlet (red curve) with isomer shift $\delta_T \approx 1.92(2)$ to $1.98(2) \text{ mm/s}$ range, and a doublet (blue curve) with an isomer shift, $\delta_{\text{DO}} \approx 3.17(2)$ to $3.24(2) \text{ mm/s}$ range, and a quadrupole splitting of $\Delta \approx 0.73(3)$ to $1.08(3) \text{ mm/s}$ range, but with observed linewidths, $\Gamma \approx 0.94(3)$ to 1.07 mm/s suggestive of rather well-defined local environments (Table II). The singlet δ_T close to the chemical shift of c-Si (Fig. 1), is a clear indication of the presence of tetrahedral (T) coordination and sp^3 bonding, similar to what is observed in corresponding selenides [35]. The resonance doublet centered at δ_{DO} highlights the presence of Sn in octahedral sites. In contrast with a single resonance peak found in c-SnTe, in the amorphous phases one observes an electric field gradient

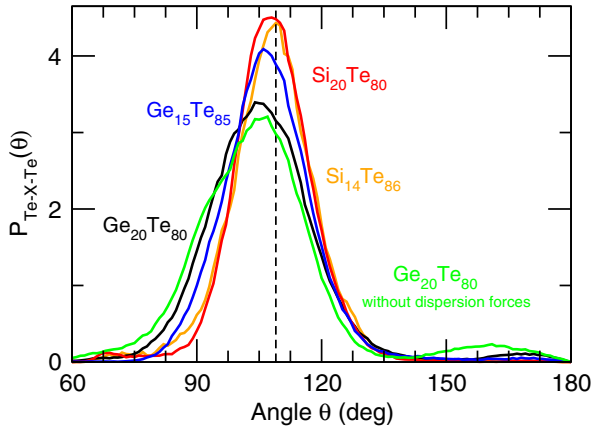


FIG. 6. (Color online) Simulated Te- X -Te ($X = \text{Ge}$ and Si) bond angle distribution in amorphous $\text{Ge}_{15}\text{Te}_{85}$, $\text{Ge}_{20}\text{Te}_{80}$, $\text{Si}_{14}\text{Te}_{86}$, and $\text{Si}_{20}\text{Te}_{80}$. The broken vertical line corresponds to the angle of 109° .

responsible for the doublet Δ , which arises from the fact that Sn is in a *defect* octahedral configuration given that a majority of Ge is fourfold coordinated (Table III and Ref. [30]). Once the integrated area of T and DO resonances is calculated, one obtains the fraction of T and DO local structures, and the fraction η_T of Ge/Si tetrahedra (Table IV).

The two binary tellurides actually display quite different behavior. In the Ge-Te glasses, the DO-pyramidal geometry, while representing minority site at $x = 15\%$, grows rapidly with increasing x and becomes the dominant motif close to $\text{Ge}_{20}\text{Te}_{80}$. This behavior is in sharp contrast to the case of the Si-based analog, which displays already a large fraction of T sites at low (14%) Si content (69.9%), and with growing x , this fraction increases mildly to 74.2% at $\text{Si}_{18}\text{Te}_{82}$. The opposite trends between Ge-Te and Si-Te alloys can be related to the known crystalline polymorphs (GeTe and Si_2Te_3) that dominate the local structure at higher modifier content, and which display for the group IV atom an octahedral and a tetrahedral environment, respectively [36,37].

B. From angular constraints

The present findings on $\eta_T(x)$ are fully consistent with those determined from models of our amorphous Ge-Te and Si-Te using the FPMD simulations, which reproduce quite accurately the experimental structure functions [30] in real space, as previously emphasized (Fig. 2). The bond angle distributions around Ge and Si (Te-Ge-Te and Te-Si-Te) already show the difference in geometry between the two systems (Fig. 6) because $\text{Si}_{14}\text{Te}_{86}$ and $\text{Si}_{20}\text{Te}_{80}$ display a distinct peak at 109° in the Te-Si-Te bond angle distribution, indicative of the tetrahedral geometry. However, both $\text{Ge}_{15}\text{Te}_{85}$ and $\text{Ge}_{20}\text{Te}_{80}$ have their bond angle distribution shifted to lower angles (95° – 100°), together with a small contribution at 160° , which indicate a predominantly DO geometry for Ge. One furthermore notes that the absence of dispersion forces [see Eq. (1)] leads to an increased contribution at 160° (green curve, Fig. 6), as discussed below. As already noticed before [10,11], these “global” bond angle distributions do not permit accessing the precise population of tetrahedra.

To detect and calculate quantitatively their population, we use algorithms that enumerate angular topological constraints, but in contrast with a previous work [38], we do not perform an initial search of tetrahedral units using a bond length argument [11], and fully rely on angular excursions that are computed on-the-fly. We follow individually over the simulation trajectory the $N_a = N(N-1)/2$ angles defined by a set of N first neighbors around a central Ge or Si atom (in the following, we choose $N = 6$). Over the simulated trajectory (i.e., with time), these individual angles define a partial bond angle distribution out of which a mean $\bar{\theta}$ and a standard deviation σ_θ can be computed for *each* Ge/Si atom of the system. If the number of low standard deviations σ_θ around an atom is six, a tetrahedron is identified because this geometry is defined by six rigid angles [39] that give rise to corresponding low angular standard deviations [Fig. 7(a)]. In this respect, this dichotomic selection rule differs from previous methods that rely on continuous structural parameters. Averaging over the system then leads to a precise fraction η_T of Ge or Si tetrahedra that compares favorably to the experimental estimate (Table IV). Once the six angular excursions are identified, Fig. 7(b) shows indeed that the associated system-averaged mean angles are equal to $\langle \bar{\theta} \rangle \simeq 109^\circ$ (blue arrows), and a corresponding bond angle distribution [Fig. 7(c)] peaks at 109° . Both Si-Te and Ge-Te systems display a similar distribution, the latter being identical to the corresponding Se-Ge-Se distribution [39] in the isovalent $\text{Ge}_{20}\text{Se}_{80}$ where $\eta_T = 100\%$. The similarity between the Si- and Ge-based bond angular distribution of T sites is also consistent with the identical isomer shift δ_T found in Mössbauer spectroscopy [red curves in Figs. 5(a) and 5(b)] for $\text{Ge}_x\text{Te}_{1-x}$ and $\text{Si}_x\text{Te}_{1-x}$.

The remaining nontetrahedral (nT) Ge and Si geometry can now also be characterized. In $\text{Ge}_{20}\text{Te}_{80}$, only three angles are found to have small angular excursions ($\sigma_\theta \simeq 10^\circ$ – 17° , red bars/angles for ${}_1\text{Ge}_2(n=1)$, ${}_1\text{Ge}_3(n=2)$, and ${}_2\text{Ge}_3(n=6)$, Fig. 7(a), and are associated with the first three neighbors of Ge at distances of about $2.69 \pm 0.07 \text{ \AA}$, and with angles found at $\bar{\theta} \simeq 98^\circ$ [red arrows, Fig. 7(b)]. This defines a pyramid with a triangular basis having the Te-Te bonds as edges, and a Ge at the remaining vertex, similar to the pyramidal geometry found in As_2Se_3 for which three rigid angles are also obtained [40]. This leads to a similar bond angle distribution [orange curve, Fig. 7(c)]. However, in the first coordination shell, a fourth neighbor (Te) is found at a slightly larger distance (2.96 \AA), and the associated angles [${}_1\text{Ge}_4(n=3)$, ${}_2\text{Ge}_4(n=7)$ and ${}_3\text{Ge}_4(n=10)$] exhibit much larger angular excursions [25° – 35° , red bars/angles 3, 7, and 10, Fig. 7(a)] indicating a much softer geometry with corresponding angles found at 105° – 115° [Fig. 7(b)]. We recover similar results for the remaining $\text{Ge}_{10}\text{Te}_{90}$, $\text{Ge}_{15}\text{Te}_{85}$, and $\text{Si}_{14}\text{Te}_{86}$.

V. DISCUSSION

Having established the fraction η_T of such sp^3 tetrahedral structures, we then address the question of their occurrence with decreasing temperature. An investigation at different liquid temperatures T (923, 823, and 700 K) of $\text{Ge}_{20}\text{Te}_{80}$ shows that the fraction $\eta_T(T)$ does not track the probability $x_4(T)$ of finding a fourfold Ge, the latter being found to be 45% at 923 K, and 77% at 300 K. We find tetrahedra represent

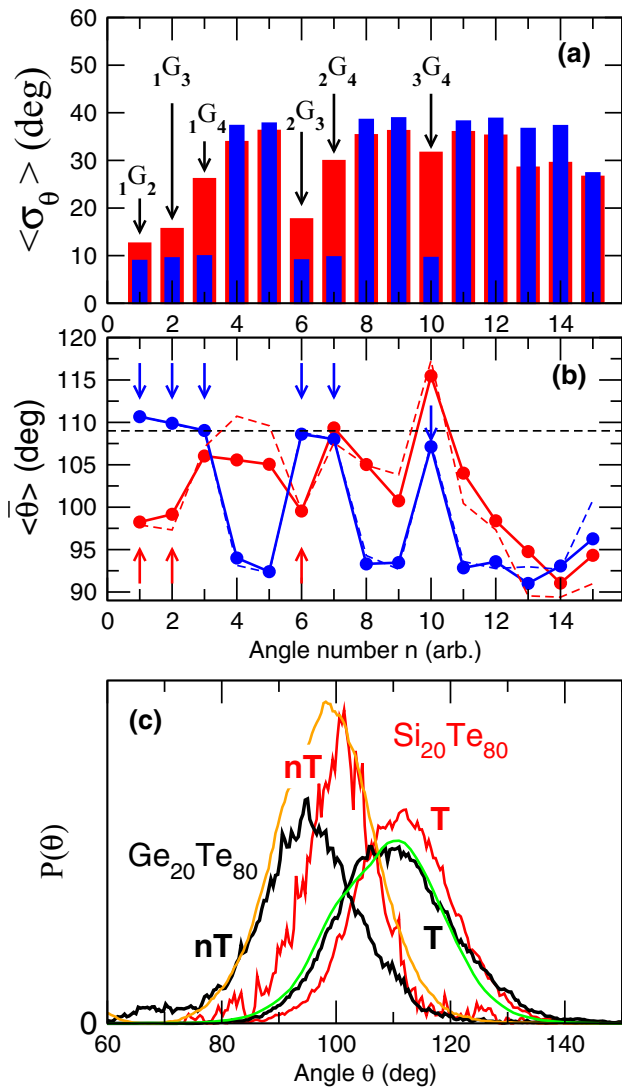


FIG. 7. (Color online) (a) Standard deviation $\langle \sigma_\theta \rangle$ for arbitrary angle numbers n ($0 < n < N_a = 15$) around Ge atoms in amorphous $Ge_{20}Te_{80}$ split into two categories: Ge atoms having six low σ_θ 's (blue), and Ge atoms having not such six σ_θ 's (red). Brackets indicate system averages. The arrows indicate the relevant angles ${}_k G_m(n)$ serving for the discussion. Here, m and $k < m$ are the Te neighbors, and labeled according to their distance with respect to the central Ge atom. (b) Corresponding Ge-centred angles $\langle \bar{\theta} \rangle$. The broken lines correspond to the $Ge_{15}Te_{85}$ compound. Colored arrows indicate angles which can be considered as rigid [because of (a)] and which serve to cross-check the angles ($\approx 109^\circ$ or $\approx 98^\circ$) of the local geometries. (c) Bond angle distribution of identified tetrahedral (T)/nontetrahedral (nT) Ge and Si in $Ge_{20}Te_{80}$ (black) and $Si_{20}Te_{80}$ (red). The green curve corresponds to the $Se-Ge-Se$ bond angle distribution in the isochemical $Ge_{20}Se_{80}$ [39], and the orange curve corresponds to the simulated $Se-As-Se$ bond angle distribution of pyramidal As in amorphous As_2Se_3 [40].

minority sites at 923 K (20%) but then their concentration steadily increases at room temperature where they represent the dominant motif (54.6%, Table IV).

Given the high content of tetrahedra for this compound [Fig. 5(a) and Table IV], an immediate consequence of the present findings is that changes in bonding and geometri-

cal motifs should definitely play an important role in the phase-change phenomenon. First, the conclusion traces back to a proposed mechanism [3] for the crystal-amorphous transition, related to the local switching (an “umbrella-flip”) of Ge atoms from an octahedral to a tetrahedral environment. This picture has been challenged in the literature from FPMD simulations disregarding dispersion forces but such simulations (as the green curve in Fig. 6) usually lead to a systematic overestimation of the Ge-Te bond lengths and Ge coordination numbers with respect to experiments [30] as also revealed in the liquid phase [29]. They also lead to a significantly higher fraction of octahedra as we have calculated $\eta_T = 23.4\%$ for $Ge_{20}Te_{80}$ without Eq. (1), which also manifests in a different shape for the total bond angle distribution [green curve, Fig. 2(b)] and an increased contribution around 160° . Simulations with dispersion corrections (black curves in Fig. 2) exhibit an increased agreement with experiments, and lead to reduced bond lengths thus promoting an increased tetrahedral bonding, a feature quite well established when bond lengths are followed during a controlled tetrahedral to octahedral conversion under pressure [41].

The determined bonding characteristics leads to even broader consequences. With an average number of (s,p) electrons usually larger than four, sp^3 hybridization in phase-change materials seems unlikely at a first glance. Indeed, sp^3 tetrahedral geometries would involve occupied (but energetically unfavourable) sp^3 antibonding states, and lead to the absence of resonance bonding which seem to control [42] a certain number of electronic properties (e.g., contrast) for phase-change applications. This seems consistent with the fact that the ease of phase switching is directly linked to small ionicity and a limited degree of hybridization [1], enabling resonance p -electron bonding to prevail. However, given the observed large number of sp^3 hybridization found in the present Ge-Te binary, one is led to believe that only a fraction $(1 - \eta_T)$ of Ge atoms must be involved in such p -bond driven phase-change mechanism. While we cannot further comment on popular phase-change alloys (e.g., GeTe or $Ge_2Sb_2Te_5$) given our investigated compositions, because of a large fraction of Ge being in sp^3 hybridized, only select number of atoms must obviously be subject to resonance bonding in order to drive the properties of, e.g., the $Ge_{20}Te_{80}$ compound which has been found to exhibit [43] more promising switching temperatures (crystallization/melting) when compared with GeTe or the GST225, indicating that it may also be a competitive candidate for memory applications.

VI. SUMMARY AND CONCLUSIONS

In this paper, we coupled aspects of local structures from Mössbauer spectroscopy with those determined from DFT using dispersion forces—a totally new accomplishment that has not been done previously in the field of disordered solids, both numerically and experimentally.

There exist numerous structural investigations of phase-change materials, and many of them have been reported in the literature, from, e.g., neutron diffraction [6,12,30,31], x-ray diffraction [3,5], Raman [13] or photoemission spectroscopy [9]. However, none of them allows to probe the local structure in a quantitative fashion. In itself, the use of ^{119}Sn Mössbauer spectroscopy represents a major step forward

for the structural characterization of Ge or Si local sites in amorphous tellurides by evaluating the fraction of tetrahedra without any ambiguity. Determining accurately the tetrahedral fraction in such materials is certainly neither a side issue in the field, nor a more technical one, it is at the center. While it is well known that in the lighter alloys (Ge-O, Ge-S, Ge-Se), Ge acquires a 100% tetrahedral coordination [39,41], not much is known about the Ge coordination in the heavier tellurides (GST, Ge-Te, . . .) so that the nature of chemical bonding in such materials is an open question, and is much debated today, given the obvious technological implications.

In contrast with other experimental techniques, Mössbauer leads to a clear signal of the local symmetry including geometry, tetrahedral versus octahedral, and permits determining exactly the fraction of tetrahedra. This technique yields a higher correlation of structure, not just bonds, but how these bonds are locally configured (tetrahedrally or octahedrally). The nuclear hyperfine signals are directly transferable to those in reference compounds which exhibit either a purely tetrahedral structure (crystalline Si) or a purely octahedral structure (crystalline SnTe). The technique once applied can be extremely powerful as the present work and earlier work in the field of glasses has demonstrated [17]. The present work has demonstrated that the tetrahedral fraction is large, at about 57% for Ge₁₅Te₈₅, and consistent in a neat way with MD calculations of that fraction. The numerical estimate is based on angular topological constraints, an original method which slightly differs from previous work [38].

The results may furthermore provide some credit to the umbrella-flip model [3] where a large number of tetrahedra are present in the amorphous phase. It has indeed been proposed that the nature of the crystal to amorphous phase

transition, which resides at the core of the phase-change phenomenon and data storage, is driven by a structural change from an octahedral Ge coordination (in the crystal phase) to a tetrahedral Ge one in the amorphous phase. Thus the question of “*how many tetrahedra, if any ?*” appears, therefore, to be central, and crucial for the field. The tetrahedral Ge fraction in Ge-Te is very difficult to estimate given that only indirect evidences can be provided by Raman or x-ray photoemission spectroscopy. DFT simulations which usually disregard dispersion forces, lead to structural models that exhibit a “*bond-distance*” problem [12,29], i.e., Ge-Te bond distance lengths longer than the experimental measured ones. Longer bond lengths may erroneously lead to an increased fraction of octahedral Ge species. This is a well-known feature reported in pressure induced tetrahedral to octahedral conversion of glasses [41]. These numerical flaws have led to a series of studies challenging the umbrella model, given that the qualitative [11–13] DFT computed fraction of tetrahedra is actually quite low. The present contribution closes the debate by providing a quantitative estimate, both theoretically and experimentally, and also demonstrates that DFT simulations without dispersion forces lead to a fraction of tetrahedra that is erroneously low.

ACKNOWLEDGMENTS

M.M. acknowledges support from Agence Nationale de la Recherche (ANR) (Grant No. ANR-11-BS08-0012), from the Franco-American Fulbright Commission, and International Materials Institute. P.B. acknowledges support from NSF grant DMR-08-53957. Mathieu Bauchy and Daniel Skoncz-Traintz are gratefully acknowledged for stimulating discussions.

-
- [1] T. Hickel, J. Neugebauer, M. Wuttig, D. Lencer, M. Salinga, and B. J. Grabowski, *Nat. Mater.* **7**, 972 (2008).
- [2] *Phase Change Materials and Applications*, edited by S. Raoux and M. Wuttig (Springer, Berlin, 2008).
- [3] A. V. Kolobov, P. Fons, A. I. Frenkel, A. L. Ankudinov, J. Tominaga, and T. Uruga, *Nat. Mater.* **3**, 703 (2004).
- [4] A. V. Kolobov, P. Fons, and J. Tominaga, *Appl. Phys. Lett.* **82**, 382 (2003).
- [5] D. A. Baker, M. A. Paesler, G. Lucovsky, S. C. Agarwal, and P. C. Taylor, *Phys. Rev. Lett.* **96**, 255501 (2006).
- [6] S. Kohara *et al.*, *Appl. Phys. Lett.* **89**, 201910 (2006).
- [7] K. Gunasekera, S. Bhosle, P. Boolchand, and M. Micoulaut, *J. Chem. Phys.* **139**, 164511 (2013).
- [8] P. Jónvári, I. Kaban, J. Steiner, B. Beuneu, A. Schöps, and M. A. Webb, *Phys. Rev. B* **77**, 035202 (2008).
- [9] M. Krbal, A. V. Kolobov, P. Fons, J. Tominaga, S. R. Elliott, J. Hegedüs, and T. Uruga, *Phys. Rev. B* **83**, 054203 (2011).
- [10] J. Akola and R. O. Jones, *Phys. Rev. B* **76**, 235201 (2007).
- [11] J.-Y. Raty, C. Otjacques, J. P. Gaspard, and C. Bichara, *Solid State Sci.* **12**, 193 (2010).
- [12] J. Kalikka, J. Akola, R. O. Jones, S. Kohara, and T. Usuki, *J. Phys. Cond. Matt.* **24**, 015802 (2012).
- [13] S. Caravati, M. Bernasconi, T. D. Kuehne, M. Krack, and M. Parrinello, *Appl. Phys. Lett.* **91**, 171906 (2007).
- [14] P. L. Chau and A. J. Hardwick, *Mol. Phys.* **93**, 511 (1998).
- [15] R. Mazzarello, S. Caravati, S. Angioletti-Uberti, M. Bernasconi, and M. Parrinello, *Phys. Rev. Lett.* **104**, 085503 (2010).
- [16] M. Krbal, A. V. Kolobov, P. Fons, K. V. Mitrofanov, Y. Tameroni, J. Hegedüs, S. R. Elliott, and J. Tominaga, *Appl. Phys. Lett.* **102**, 111904 (2013).
- [17] P. Boolchand, in *Physical Properties of Amorphous Materials*, edited by D. Adler, B. B. Schwartz, M. C. Steele (Plenum Press, New York, 1985), p. 221.
- [18] S. Bhosle, K. Gunasekera, P. Boolchand, and M. Micoulaut, *Intl. J. of Appl. Glass Sci.* **3**, 189 (2012).
- [19] S. Bhosle, K. Gunasekera, and P. Boolchand, *Intl. J. of Appl. Glass Sci.* **3**, 205 (2012).
- [20] K. Gunasekera, P. Boolchand, and M. Micoulaut, *J. Appl. Phys.* **115**, 164905 (2014).
- [21] S. Chakraborty and P. Boolchand, *J. Phys. Chem. B* **118**, 2249 (2014).
- [22] M. K. Gauer, I. Dézsi, U. Gonser, G. Langouche, and H. Ruppertsberg, *J. Non-Cryst. Solids* **101**, 31 (1988).
- [23] R. Car and M. Parrinello, *Phys. Rev. Lett.* **55**, 2471 (1985).
- [24] Y. Tsuchiya, *J. Non-Cryst. Solids* **312–314**, 212 (2002).
- [25] Y. Tsuchiya, *J. Non-Cryst. Solids* **136**, 37 (1991).
- [26] J. Akola, R. O. Jones, S. Kohara, T. Usuki, and E. Bychkov, *Phys. Rev. B* **81**, 094202 (2010).
- [27] S. Grimme, *J. Comput. Chem.* **27**, 1787 (2006).
- [28] M. Micoulaut, *J. Chem. Phys.* **138**, 061103 (2013).

- [29] M. Micoulaut, M.-V. Coulet, A. Piarristeguy, M. Johnson, C. J. Cuello, C. Bichara, H. Flores-Ruiz, and A. Pradel, *Phys. Rev. B* **89**, 174205 (2014).
- [30] P. Jóvári, A. Piarristeguy, R. Escalier, I. Kaban, J. Bednarcik, and A. Pradel, *J. Phys. Cond. Matt.* **25**, 195401 (2013).
- [31] I. Kaban, Th. Halm, W. Hoyer, P. Jövari, and J. Neufeind, *J. Non-Cryst. Solids* **326-327**, 120 (2003).
- [32] F. Kakinuma, T. Fukunaga, and K. Suzuki, *J. Non-Cryst. Solids* **312-314**, 380 (2002).
- [33] L. Rátkai, A. P. Gonçalves, G. Delaizir, C. Godart, I. Kaban, B. Beneu, and P. Jóvári, *Solid St. Comm.* **151**, 1524 (2011).
- [34] C. Massobrio, M. Celino, P. S. Salmon, R. A. Martin, M. Micoulaut, and A. Pasquarello, *Phys. Rev. B* **79**, 174201 (2009).
- [35] P. Boolchand, P. Chen, M. Jin, B. Goodman, and W. J. Bresser, *Physica B* **389**, 18 (2007).
- [36] S. Raoux, W. Welnic, and D. Ielmini, *Chem. Rev.* **110**, 240 (2010).
- [37] K. Ploog, W. Stetter, A. Nowitzki, and E. Schönherr, *Mater. Res. Bull.* **11**, 1147 (1976).
- [38] M. Micoulaut, J.-Y. Raty, C. Otjacques, and C. Bichara, *Phys. Rev. B* **81**, 174206 (2010).
- [39] M. Micoulaut, A. Kachmar, M. Bauchy, S. Le Roux, C. Massobrio, and M. Boero, *Phys. Rev. B* **88**, 054203 (2013).
- [40] M. Bauchy and M. Micoulaut, *J. Non-Cryst. Solids* **377**, 34 (2013).
- [41] J. P. Itié, A. Polian, G. Calas, J. Petiau, A. Fontaine, and H. Tolentino, *Phys. Rev. Lett.* **63**, 398 (1989).
- [42] K. Shportko, S. Kremers, M. Woda, D. Lencer, J. Robertson, and M. Wuttig, *Nat. Mater.* **7**, 653 (2008).
- [43] H. Jiang, K. Guo, H. Xu, Y. Xia, K. Jiang, F. Tang, J. Yin, and Z. Liu, *J. Appl. Phys.* **109**, 066104 (2011).